Chapter 5

Swirl-Inducing Ducts

Trevor Frank Jones

Additional information is available at the end of the chapter

http://dx.doi.org/10.5772/intechopen.78959

Abstract

This chapter examines the flow of swirling liquid in a duct. In many cases, circumferential velocity in the cross-section of a cylindrical duct is a remarkably linear function of radius up to the proximity of the duct wall. This is similar to the behaviour of a twisting solid shaft and the analogy leads to a *solid body model* for swirl flow in ducts. Helically profiled lobate duct walls provide a twisting torque, while wall friction in simple circular ducts causes swirl to decay. The liquid counterpart of the solid body is represented as a first-order system in downstream distance because of the way torque is transmitted by duct walls rather than by shaft stiffness as in the solid case. The effect of the inertia of the rotating and twisting cylinder is unchanged from its solid counterpart, and damping is related to the viscosity of the liquid acting over the annulus between the rotating liquid cylinder and the duct wall. The shear stress in the liquid is shown to be linearly related to the intensity of the swirl. The generation of swirl is briefly described with reference to lobate designs, their development of shape and helix.

Keywords: swirl, solid-liquid pipeflow, slurry transport, computational fluid dynamics

1. Introduction

Why impart swirling flow to a stream of fluid? Spanner, a much respected naval architect, invented a helical lobate tube which increased the efficiency of heating of water in the boilers of ships [1, 2]. Importantly, his design could be manufactured economically by drawing cylindrical tube through special dies (see **Figure 1**).

For particle-bearing liquids, swirl puts particles into suspension at lower axial velocities than would be the case for a cylindrical duct. Once in suspension, particles (or debris for down-stream collection) remain in full or partial suspension long after the swirl has decayed to negligible proportions.

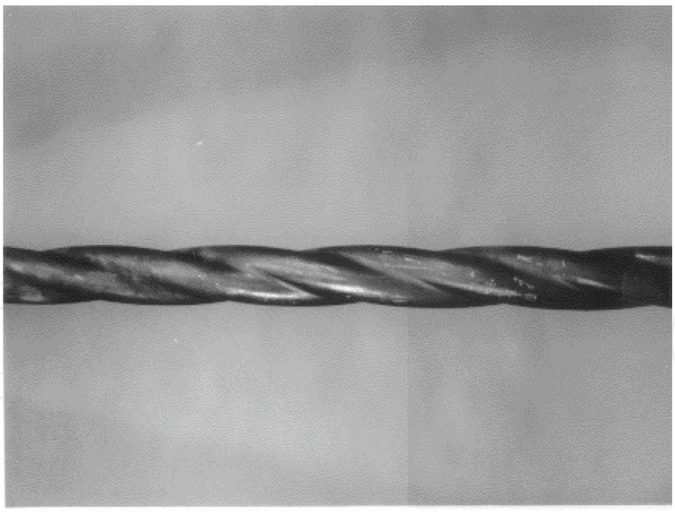

Figure 1. Three-lobe boiler tube after Spanner, 1939, 1945. Reproduced courtesy of Transport and Sedimentation Conference, Wroclaw University of Environmental and Life Sciences, Poland.

Lower axial velocity implies much lower pumping power: a strong economic reason to swirl the flow in the first place. The efficacy of swirl generation in pumping particulate liquids, particularly river slurries, has been recognized for many years. The Gordon patent for a duct with internal vanes to encourage swirl was published in 1899 [3].

Economic benefits are not the only reasons for studying swirl. In some instances, enhanced swirl is required irrespective of increased pressure losses and pumping power requirement.

The data in this chapter originate from several sources. Much of it comes from validated computational fluid dynamics (CFD) code using RANS (Reynolds-averaged Navier Stokes equations). The basis of these equations is 'Reynolds decomposition', whereby an instantaneous quantity is decomposed into time-averaged quantities and fluctuating quantities. In cylindrical polar co-ordinates (r,θ,z), the time-averaged velocities are u, v and w and the fluctuating velocities are u', v' and w'. In essence, the fluctuating quantities can be assumed to have a temporal mean of zero. This makes for an increase in the number of unknowns because the cross products ($\overline{u'u'}$, $\overline{v'v'}$, $\overline{w'w'}$, $\overline{u'v'}$, $\overline{u'w'}$, and $\overline{v'w'}$) have to be determined.

RANS turbulence modelling techniques are often classed by the number of equations used to model the flow field. Early results were obtained using two-equation $(k-\epsilon)$ and $(k-\omega)$ models, where k represents the turbulent kinetic energy, ϵ represents the rate of dissipation of turbulent energy and ω represents the specific rate of dissipation of turbulent kinetic energy into internal thermal energy. As greater computer power became available, the six-equation Reynolds stress model (RSM) became the method of choice for swirling flows. There are variations in RSM solutions. The CFX RSM-ω [5] has been used since it can give more accuracy near the wall.

2. Characterizing swirl

Firstly, I should explain what I mean by 'swirl' and then define precise ways to assess it. In turbulent pipe flow, there are many eddies and circulations cascading from the large to the

small. Kolmorogov [6] showed that most of the kinetic energy in the flow is contained in large-scale structures. Energy 'cascades' to smaller scales by an inviscid mechanism until it is small enough for viscous dissipation to take place. I define swirl as large-scale, one-way circulation surrounding the geometric centre of the duct.

With a definition of swirl in place, I now need to explain the mathematical measures of this behaviour. Is it useful, strong or weak, efficient or profligate in its expenditure of pipeline pressure? The first and most obvious measure is the circumferential velocity, sometimes referred to as tangential velocity, w_{max}, taken at its maximum in the cross-section. Useful in itself, this direct measure is important in application to downstream devices—cyclones or pumps for example.

Circumferential velocity as a measure of swirl takes no account of the axial velocity required to generate or maintain it. In contrast, the *swirl angle*, incorporating the axial velocity, indicates the angular deflection of the flow and can be clearly seen in transparent pipe sections (see **Figure 2**). Tonkin [7] used these images to infer tangential velocity for a series of particle concentrations and axial velocities.

The *swirl angle*, θ_S, is given by

$$\theta_S = \tan^{-1} \frac{w_{max}}{u_m} \tag{1}$$

where u_m is the mean axial pipe velocity.

Measurement transducers can be corrupted by swirling flow, and International Standard ISO 5167 specifies a maximum swirl-angle limit of 2° at or near transducer stations.

The swirl angle does not take account of the angular momentum given to the flowing liquid. The ratio of angular momentum flux to the product of pipe radius and axial momentum flux is known as the *swirl intensity* or *swirl number*, Ω. (Note that a simple ratio of angular to axial

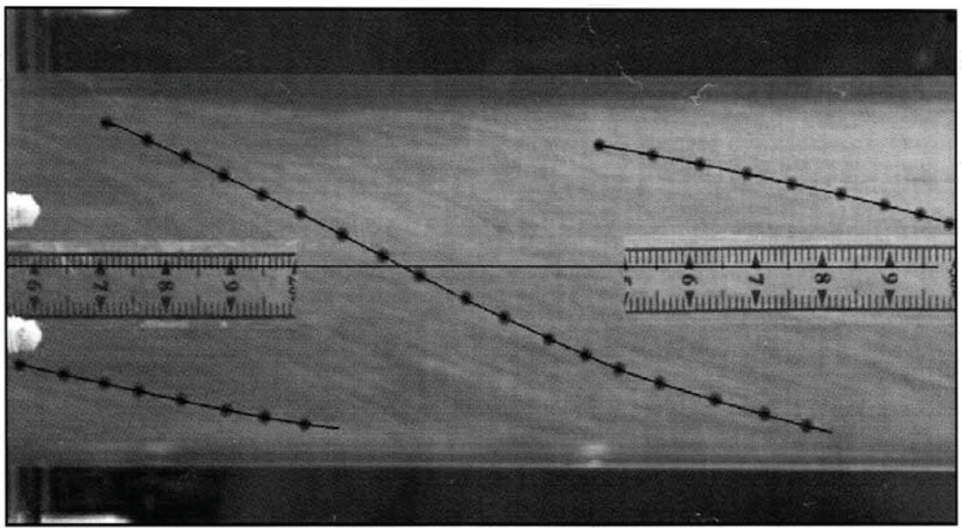

Figure 2. 1.4% by volume coarse sand in water, axial velocity 1.7 m/s showing *swirl angle*. Image from Tonkin [7] with thanks.

momentum would not be dimensionless.) There are several versions of this definition and the version defined in Eq. (2) allows for variations in the axial velocity with radial displacement.

$$\Omega = \frac{2\pi\rho \int_0^R uwr^2 dr}{R \times 2\pi\rho \int_0^R u^2 r dr} = \frac{\int_0^R uwr^2 dr}{R \int_0^R u^2 r dr} \tag{2}$$

where R is the pipe bore radius (of the cylindrical delivery pipe), u is the axial velocity at radius r, and w is the circumferential velocity at radius r.

Swirl number gives a simple way to classify swirl for computational calculation methods. If $\Omega < 0.5$, two-equation methods (such as $(k-\epsilon)$ and $(k-\omega)$) are generally considered adequate. If $\Omega \geq 0.5$, the six-equation RSM is preferred despite the increased computational cost.

Swirl intensity and swirl angle are closely related measures and in many cases an almost linear relation exists between them.

Pressure loss is an inevitable consequence of swirl generation and it is important to use that pressure effectively. Ganeshalingam [8] developed a dimensionless group, *swirl effectiveness*, S, given by

$$S = \frac{\Omega}{\frac{\Delta P}{\frac{1}{2}\rho u^2}} \tag{3}$$

where ΔP is the pressure loss over a length of duct and ρ is the fluid density.

This measure has proved invaluable in optimizing Spanner-type duct designs.

Another pressure-related metric for use when a Spanner-type duct generates swirl is the pressure loss for an equivalent length of smooth circular tube. The well-known Darcy-Weisbach equation can be used to calculate this:

$$\Delta P_s = f \frac{L}{D} \frac{\rho u^2}{2} \tag{4}$$

where f is the friction factor for a smooth duct, L is the duct length and D is the duct diameter. A simple ratio can be used to gauge the magnitude of the pressure loss suffered as a result of the use of the duct:

$$\textit{Pressure penalty factor} = \frac{\Delta P}{\Delta P_s} \tag{5}$$

3. The solid body model

In many cases of developed swirling flow, the swirl angle, θ, is found to be almost constant over most of the cross-section. **Figure 3** shows a tangential velocity profile for a nominal axial velocity

http://dx.doi.org/10.5772/intechopen.78959

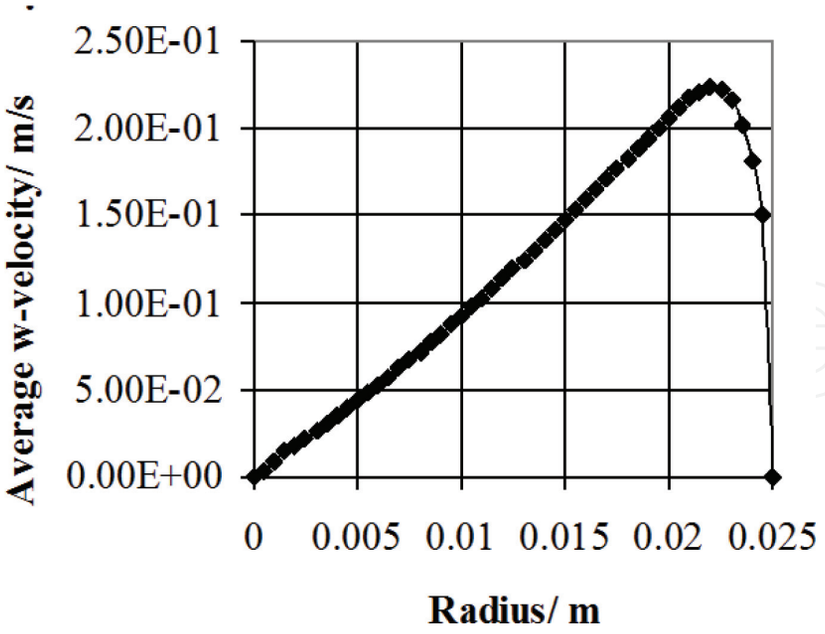

Figure 3. Circumferential velocity, *w,* downstream of a three-lobe swirl-inducing duct similar to Spanner's design. Data from Raylor with thanks.

of 2 m/s. The near linearity over approximately 84% of the bore also indicates that angular velocity, ω, is similarly constant in this range. Constant angular velocity is a characteristic of a solid rotating shaft and this concept suggests a simple mechanical analogy of *the solid body model* which can be used to describe swirling flow.

Damping friction (directly proportional to tangential velocity) clearly has little effect in the central 84% of **Figure 3**. The peripheral 16% of the velocity profile indicates gathering damping friction as the radius increases. At the outer radial extremity, the circumferential velocity falls to zero in accordance with the *no-slip* principle of Newtonian mechanics. This outer damping annulus is characterized by a dimensionless distance from the wall, with y^+ defined as

$$y^+ = \frac{u_* y}{\nu} \tag{6}$$

where u_* is the friction (shear) velocity $= \sqrt{\frac{\tau_W}{\rho}}$, τ_w is the wall shear stress, y is the distance to the wall and ν is the kinematic viscosity.

In turbulent pipe flow, close to the wall, is a *laminar sub-layer* of width $y^+ \sim 5$. At greater distances, up to about $y^+ \sim 35$, a *buffer layer* gradually develops the laminar sub-layer into fully turbulent flow. This is much smaller than the outer 16% of **Figure 3** and later results will show that the solid body starts at approximate distance $y^+ \sim 72$ for an axial velocity of 2 m/s. The distance is strongly influenced by the axial velocity. For axial velocities between 1 and 4 m/s in an industrial steel pipe of bore 50 mm, the distance to the wall can be expected to vary from about 25% to about 10% of the duct radius.

The simplified system dynamics of the analogy of a solid-liquid cylinder are described by three elements: the *inertia* of the shaft and any rotating components such as a flywheel, the *stiffness* of the shaft transmitting torque down the shaft and the *damping* of the speed of rotation. Straight away the stiffness of the shaft can be eliminated from the model. By definition, liquids do not have stiffness and they adapt to the shape of the containment without coercion. We are left with a shaft, length one pitch (for one 360° rotation), subjected to a torque M rotating at temporal rate $d\theta/dt$.

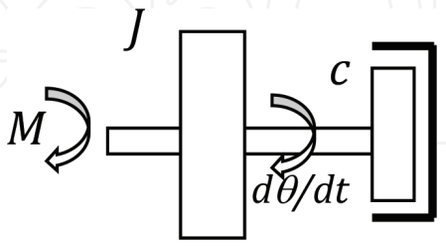

$$M = J\frac{d^2\theta}{dt^2} + c\frac{d\theta}{dt} \tag{7}$$

where J is the polar second moment of mass of the cylinder and c represents a damping coefficient dependent upon the area of the shearing surfaces. The torque moment M can be positive for a Spanner-type pipe or can approach zero for a frictionless cylindrical tube.

In the model, the coefficient of damping, c, is provided by the viscosity of the liquid. Consider fully developed swirling flow in the core of a cylindrical duct (**Figure 4**). In the example above (mean axial velocity = 2 m/s), there is a zone of approximate width y^+ = 72 in which all the

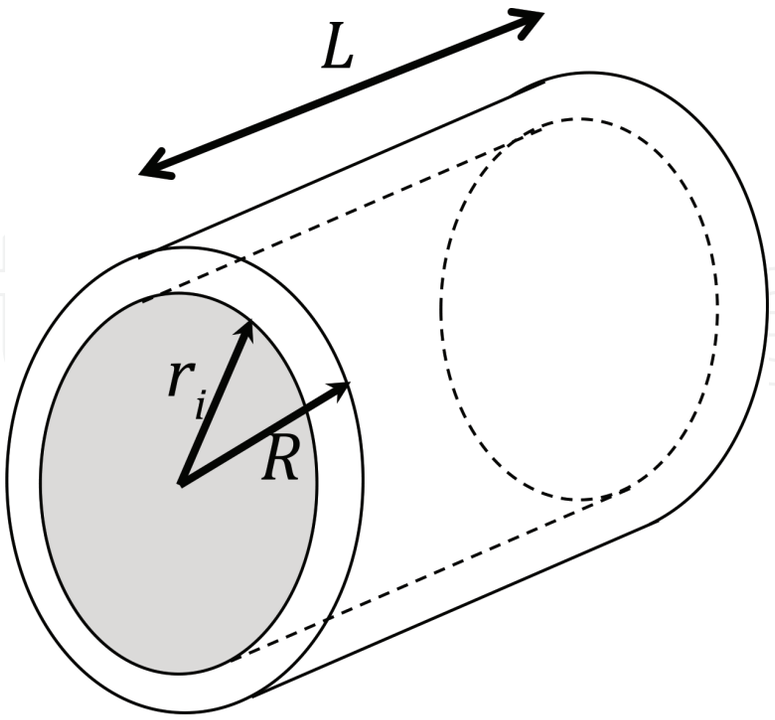

Figure 4. Fully developed swirling flow in a cylindrical duct.

damping occurs. Note that if the swirl is generated by a Spanner-type duct, there will be other shearing surfaces in the core flow where the rotating annuli meet the as yet non-rotating central portion. This is sometimes referred to as a *wall-jet* profile (Steenbergen and Voskamp [9]).

In order to quantify the damping coefficient, c, I concentrate on the viscous part of Eq. (7). Put another way, I assert $\frac{d^2\theta}{dt^2} \rightarrow 0$ for the time being.

$$M_{viscous} = c\frac{d\theta}{dt} \tag{8}$$

Newton's law of viscosity gives

$$\tau = \mu\frac{du}{dy} \approx \mu\frac{r_i\frac{d\theta}{dt}}{(R - r_i)} \tag{9}$$

Torque is applied at the outer radius as wall friction or reaction from the pipe profile, so

$$\frac{M_{viscous}}{2\pi RL} = \mu\frac{r_i\frac{d\theta}{dt}}{(R - r_i)} \tag{10}$$

Comparing (10) with (8), we obtain the coefficient of damping per unit length.

$$\frac{c}{L} = \mu\frac{2\pi Rr_i}{(R - r_i)} = \mu\frac{2\pi R(R - y)}{y} \tag{11}$$

where y is the distance from the wall of the duct.

The next major challenge to the solid body model is the transmission of torque. In a solid shaft, the torque is transmitted by its stiffness, but stiffness has been discounted as a factor in liquids. In the case of a profiled swirl tube, the torque comes from the interaction of the axial flow with the walls of the tube, an interaction the author describes as the *driving function*. This becomes clear when Eq. (7) is rewritten so that the dependent variable becomes axial distance along the cylinder (z). Putting G = twist gradient $d\theta/dz$

$$M = J\frac{d^2\theta}{dz^2}\left(\frac{dz}{dt}\right)^2 + c\frac{d\theta}{dz}\left(\frac{dz}{dt}\right) = J\frac{dG}{dz}u^2 + cGu \tag{12}$$

Dividing throughout by cu

$$\frac{M}{cu} = G_D(z) = \frac{Ju}{c}\frac{dG}{dz} + G \tag{13}$$

Note that the group of variables at the left-hand side of Eq. (3) $G_D(z) = \frac{M}{cu}$ has the same dimensions as G and is the *driving function*, i.e.

$$Tu\frac{dG}{dz} + G = G_D(z) \tag{14}$$

where the time constant

$$T = \frac{J}{c} \tag{15}$$

The *complementary function*, or transient $G_{cf}(z)$, is the solution to $Tu\frac{dG}{dz} + G = 0$. This has the form

$$G_{cf}(z) = Be^{-\frac{z}{Tu}} \tag{16}$$

The solution to Eq. (14) has another (steady-state) part, the *particular integral* (PI), $G_{pi}(z)$, which depends on the driving function $G_D(z)$. The total response is a combination of these two components

$$G(z) = G_{cf}(z) + G_{pi}(z) \tag{17}$$

There are a series of driving functions of interest and I shall start with the simplest: the decay of swirl angle downstream of swirling flow from, for example, a pump output or double elbow. The driving function $G_D(z)$ in this case is a negative step change from the initial swirl angle to zero.

When $z = 0$, $G(z) = G_o$, the initial swirl gradient. Eq. (16) gives

$$B = G_o \; i.e. \; G(z) = G_o e^{-\frac{z}{Tu}} \tag{18}$$

Halsey [10] studied the swirl in clean water following a double elbow. His work was aimed at measurement devices for which swirling flow is disruptive. ISO 5167 specifies a 2° swirl-angle limit for measurement purposes and Halsey came up with an empirical law for its decay as follows

$$\theta = \theta_o e^{-\frac{1.5fz}{D}} \tag{19}$$

where θ_o is the swirl angle at commencement, θ is the swirl angle at a downstream distance z, f is the friction factor and D is the diameter of the bore. Steenbergen and Voskamp [9] arrived at an almost identical equation in terms of *swirl intensity*, Ω, instead of swirl angle. Ganeshalingam's work [8] achieved close agreement with these models and a simulation exercise (below) confirms the relationships.

Differentiating (19) gives

$$\frac{d\theta}{dz} = G(z) = \theta_o\left(\frac{-1.5f}{D}\right)e^{-\frac{1.5fz}{D}} \tag{20}$$

when $z = 0$, $G_o = \theta_o\left(\frac{-1.5f}{D}\right)$, so for the Halsey model

$$\frac{G(z)}{G_o} = e^{-\frac{1.5fz}{D}} \tag{21}$$

Equating exponents in Eqs. (18) and (21), we have a first estimate of the time constant T for decay of swirl and the length of the swirling wake Tu

$$-\frac{z}{Tu} = -\frac{1.5fz}{D} \text{ from which } T = \frac{D}{1.5fu} \text{ and } Tu = \frac{D}{1.5f} \tag{22}$$

The solid body model gives us $T = \frac{J}{c}$. The polar moment of inertia, J, of a solid cylinder, density ρ, per unit length (L) is given by

$$\frac{J}{L} = \frac{1}{2}\rho\pi\left(\frac{D}{2}\right)^4 \tag{23}$$

From this, and the time constant T, a value of c/L can be deduced which can be used with Eq. (11) to estimate the distance, y, of the solid body from the wall of the duct.

It is not possible to specify the total extinction of swirl. For some purposes, the point of 95% reduction in swirl angle (L_{95}) after a downstream distance of $3Tu$ should be a useful approximation. If swirl is a desirable property (to keep solids in suspension for example), the *half-life* distance ($L_{50} = 0.6931 \times (Tu)$) is a more appropriate concept. **Table 1** tabulates these calculations for a series of axial velocities and indicates that the level of swirl at Reynolds number of 100,000 in an industrial steel pipe with friction factor 0.022 can be assumed to have decayed to half its initial value after about 21 diameters using the solid body model.

It is generally accepted that a y^+ value of about 35 indicates the edge of the buffer layer next to the wall. The range of values of y^+ significantly greater than this value suggests that there is an annulus of turbulent flow between the buffer layer and the solid body.

The half-life distances L_{50} are approximately constant for axial pipe velocities in the range [1.0, 4 m/s]. This is an important observation for designers of pipe systems in which the axial velocity might vary.

u	Re	f	T	L_{50}	c/L	y	y^+
m/s	**—**	**—**	**s**	**m**	**Nms/m**	**m**	**—**
1	50,000	0.024	1.37	0.95	0.00045	0.0065	82.3
1.5	75,000	0.023	0.97	1.00	0.00064	0.0050	76.8
2	100,000	0.022	0.75	1.04	0.00082	0.0040	71.8
2.5	125,000	0.022	0.61	1.06	0.00101	0.0034	67.5
3	150,000	0.022	0.52	1.07	0.00119	0.0029	63.9
3.5	175,000	0.021	0.45	1.08	0.00137	0.0026	60.8
4	200,000	0.021	0.39	1.09	0.00156	0.0023	58.0

Clean water: pipe diameter, $D = 0.05$ m; roughness height, $\varepsilon = 0.000046$ m; relative roughness, $\varepsilon/D = 0.00092$; polar moment of inertia per m, $J/L = 0.000614$ kgm^2/m.

Table 1. Solid body model: industrial steel pipe transporting clean water.

3.1. Wall shear stress in the solid body model

Starting from an analysis by Kitoh [4], the tangential momentum equation for axi-symmetric flow gives an equation for circumferential shear stress at the wall in the decay of swirl in a circular pipe.

$$\tau_{r\theta} = \rho vw + \frac{\rho}{R^2}\int_0^R r^2 \frac{\partial}{\partial z}\left(uw + \overline{u'w'} - \nu\frac{\partial w}{\partial z}\right)dr \tag{24}$$

Now $\left(uw \gg \overline{u'w'} - \nu\frac{\partial w}{\partial z}\right)$ and putting $\rho vw \to 0$, Eq. (24) for the wall can be written

$$\tau_w = \frac{\rho}{R^2}\int_0^R r^2 \frac{\partial}{\partial z}(uw)dr \tag{25}$$

where τ_W is the circumferential wall shear stress.

Leibnitz's rule for the differentiation of integrals allows the change of order of integration and differentiation in Eq. (25):

$$\tau_W = \frac{\rho}{R^2}\frac{d}{dz}\int_0^R r^2 uwdr \tag{26}$$

For a constant Reynolds number, the axial velocity $u = u_m$ is constant and the axial momentum can be simplified to a constant quantity:

$$2\pi\rho\int_0^R u^2 rdr = 2\pi\rho u_m^2\int_0^R rdr = 2\pi\rho u_m^2\frac{R^2}{2} = \pi\rho R^2 u_m^2 \tag{27}$$

This allows the simplification of swirl intensity to

$$\Omega = \frac{2\pi\rho\int_0^R r^2 uwdr}{R\times\pi\rho R^2 u_m^2} = \frac{2\int_0^R r^2 uwdr}{R^3 u_m^2} \tag{28}$$

and substituting for Ω in Eq. (26)

$$\tau_W = \frac{\rho}{R^2}\frac{d}{dz}\int_0^R\left(\frac{\Omega u_m^2 R^3}{2}\right)dr = \frac{1}{2}\rho u_m^2 R\frac{d\Omega}{dz} \tag{29}$$

i.e.

$$\frac{\tau_W}{\frac{1}{2}\rho u_m^2} = R\frac{d\Omega}{dz} = \frac{1}{2}\frac{d\Omega}{d\frac{z}{D}} \tag{30}$$

Note that since $\frac{d\Omega}{d\frac{z}{D}}$ is always negative in decaying swirl flow, values of resisting shear stress τ_W must be given a negative sign.

Returning to the analogy of a solid body for the flow, one might reasonably expect a linear relationship between circumferential stress and circumferential strain (swirl intensity or swirl

angle) for a given Reynolds number. This can be tested with a straightforward simulation experiment.

The simulation experiment (below) gives $\Omega = \Omega_0 e^{-0.0338\left(\frac{z}{D}\right)}$ for the object 50-mm smooth tube. Factoring in the measured mean friction factor yields $\Omega = \Omega_0 e^{-\xi f\left(\frac{z}{D}\right)}$ where $\xi = 1.711$.

The imposition of pipe roughness considerably increases the friction factor, f. For an axial velocity of 1.64 m/s in a commercial steel pipe (ε = 0.000046 m), friction factor is sharply increased to 0.0228. If the stress-strain assumption still holds, substituting this increased friction factor in Eq. (31) yields $-1.483f \times \Omega = \frac{d\Omega}{d\frac{z}{D}}$. The constant $\xi = 1.483$ is very close to that proposed by Steenbergen and Voskamp who achieved $\xi = 1.49 \pm 0.07$ for a larger range of values $0 \leq \Omega \leq 0.18$ [9].

SIMULATION EXPERIMENT: swirl decay in a cylindrical tube

Figure 5 shows the results of a simple RANS simulation for the flow of clean water through a 50-mm diameter smooth circular tube using the Reynolds stress model ($-\omega$ version) [5]. The entry plane is furnished with a mean axial velocity of 1.64 m/s and an initial circumferential velocity of 0.72 m/s at the wall and zero at the centre of the tube. The boundary conditions including the law of the wall are allowed to develop over an axial length of 10.0 m. The solid body model implies that wall friction will have reached 95% of its effect on the flow after $3Tu$ m and 99% after $5Tu$ m.

Reynolds number $Re = \frac{\rho u D}{\mu} = 997 \times 1.64 \times \frac{0.05}{0.001} = 81,754$

Friction factor (Blasius equation): $f = 0.3162 \times Re^{-0.25} = 0.0186$

Time constant (Eq. (22)) $T = \frac{D}{1.5fu} = \frac{0.05}{1.5 \times 0.0186 \times 1.64} = 1.09$ s

Effective range downstream: 9.5 m $\leq z \leq$ 9.98 m

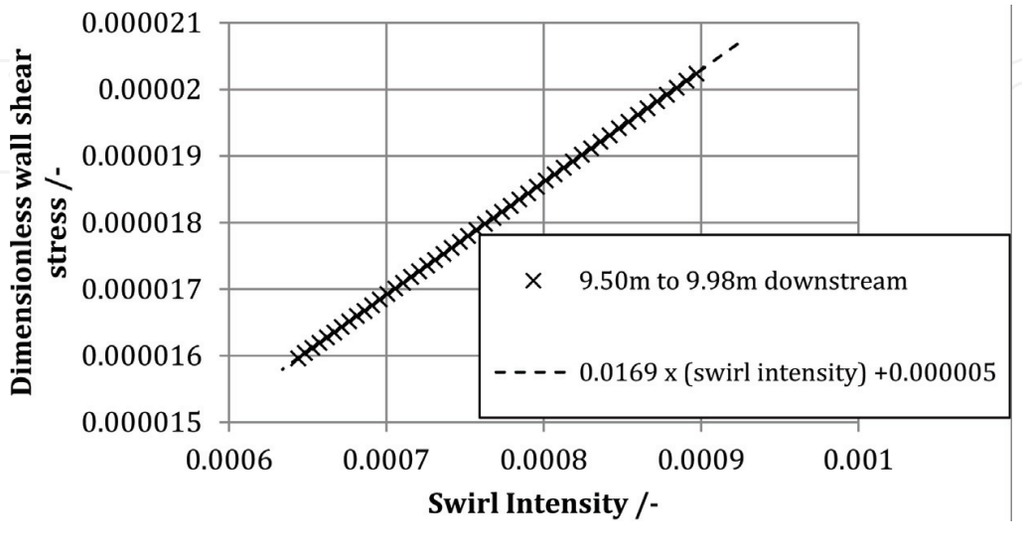

Figure 5. Dimensionless wall shear stress plotted against swirl intensity.

For the solid body model this is $5.30Tu \leq z \leq 5.57Tu$

Measured mean friction factor over range: 0.0197

In this range, the regression law applied to the CFD data is very precise ($r^2 = 0.99999$). Ignoring the small intercept as an enabling assumption,

$$-0.0169\Omega = \frac{1}{2}\frac{d\Omega}{d\frac{z}{D}} \tag{31}$$

$$\Omega = \Omega_0 e^{-k\left(\frac{z}{D}\right)} \tag{32}$$

where k = 0.0338 is a constant of proportionality and Ω_0 is the swirl intensity at outset.

Note the significant difference in time constant for smooth pipe when compared to commercial industrial steel pipe because of the increased value of the multiplier ξ. In the example, the time constant is reduced from 1.09 (smooth pipe) to 0.905 s (industrial steel pipe).

Since the swirl angle is linearly related to swirl intensity in most cases, it follows that Halsey's correlation [10] also fits the data.

4. Generating swirl

Previously, we have seen that a solid body model can be applied to the simple case of swirl decaying downstream. In these cases, the driving function is simply a step to zero: $G_D(z) \rightarrow 0$. We now come to more complex situations where the goal is to generate swirl for a specific purpose. Before addressing this problem, we must first consider the cross-sectional shape of the duct to be twisted.

The contours of duct walls should impart torque to the flow while minimizing pressure loss. By designing using this criterion, pressure costs are used in an effective way. Here, Ganeshalingham's dimensionless group, *swirl effectiveness*, S, can be used to evaluate the effectiveness of swirl generation.

$$S = \frac{S}{\frac{1}{2}\rho u^2} \tag{33}$$

4.1. Lobate designs

The boiler tube patented by Spanner and illustrated in **Figure 1** has only three lobes. Raylor [11] idealized the lobe profiles to form semicircular shapes for his CFD modelling to test the design for the transportation of particle-bearing liquids. The computer modelling was underpinned by experimental work on an extant boiler tube. Later work by Ganeshalingam showed that a four-lobe duct (or a 2-lobe duct) was more efficient when compared on the basis of swirl effectiveness.

http://dx.doi.org/10.5772/intechopen.78959

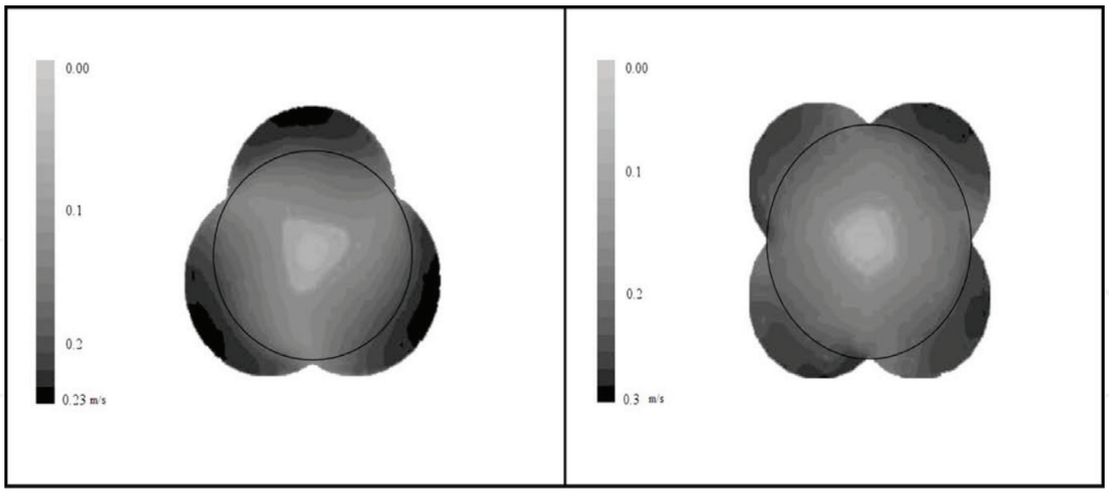

Figure 6. Contours of tangential velocity in three-lobe and four-lobe swirl pipes. Pure water with an axial velocity 2 m/s. Source: Jones and Ariyaratne [12]; reproduced courtesy: AIChE Journal.

In **Figure 6**, after Ariyaratne [13], it can be seen that the contours of tangential velocity adopt a more circular pattern in the four-lobe variant and that an efficient circulating core flow is produced in consequence.

Simply equating the area of the four-lobe duct to πR^2, the upstream area, the ratio of the lobe radius, R_4, to the upstream radius can be derived:

$$\frac{R_4}{R} = \sqrt{\frac{\pi}{2\pi + 4}} = 0.5527 \tag{34}$$

R_4 and sub-multiples have been used in other speculative swirl-duct designs so that lobe sizes can be compared across designs.

4.2. Response of the solid body model to a constant-pitch swirl duct

I first consider a four-lobe swirl duct with constant pitch:diameter ratio of 8:1 simply connected in line after a cylindrical duct. The driving function for this is a positive step or Heaviside function in swirl gradient $\frac{d\theta}{dz}$. If the imposed value of swirl gradient is G_0, this can be tried as the particular integral in Eq. (17):

$$G(z) = G_{pi}(z) + G_{cf}(z) = G_0 + Be^{-\frac{z}{Tu}} \tag{35}$$

The constant B can be easily obtained by considering the boundary condition $G(0)$ which yields $B = -G_0$. So, the solution for this case is satisfied by

$$G(z) = G_0\left(1 - e^{-\frac{z}{Tu}}\right) \tag{36}$$

Figure 7 illustrates the response of a system comprising a four-lobe Spanner-type duct with cross-sectional area equal to a cylindrical upstream main of diameter 50 mm carrying clean

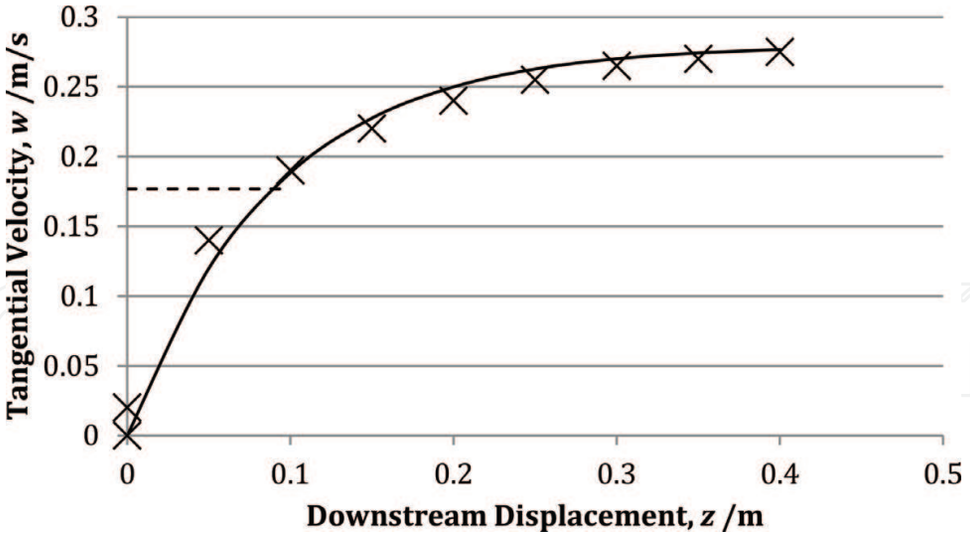

Figure 7. Response of tangential velocity in a Spanner-type swirl-inducing duct of diameter 50 mm carrying clean water at 2 m/s. Radial position is 0.7*R*. Reproduced courtesy of Transport and Sedimentation Conference, Wroclaw University of Environmental and Life Sciences, Poland.

water at an axial velocity of 2 m/s. The ordinates are tangential velocities at a radius of 0.7*R*. From these ordinates, the response of $G(z)$ can be deduced given that the twist gradient of the duct is 15.71 radians/m. Fitting Eq. (36) to these data yields $Tu = 0.1$ m. In the first-order system, 63.2% of the final value is reached after Tu metres.

The length of the wake (the point at which swirl has decayed by 95%) is $3Tu$. Hence the standard length of this four-lobe Spanner-type duct with axial velocity 2 m/s is 300 mm.

Note the apparent anomaly between the calculated constant Tu for the swirl generation case (0.1 m) and that for the swirl-decaying case from **Table 1** (1.5 m), a multiplicative factor of 15. The time constant of the model must be identical whatever driving function is applied so the only way in which this phenomenon can be explained is by studying the changes in the geometry of the rotating core for the generation case. The circumferential velocity distribution for swirl generation is a *wall jet* [9] in which circumferential velocity is concentrated towards the outer perimeter of the core flow. Effectively, the solid body in this case is not a solid cylinder, but more like a cylindrical tube. Thinking of the time constant of the system ($T = \frac{J}{c}$), the polar moment of inertia, J, is significantly reduced from that of a solid cylinder while the shearing surfaces are significantly greater than those of a solid cylinder, increasing the damping coefficient c.

4.3. Cross-section development for lobate ducts

The example of a fixed-pitch duct is useful in that it gives a standard length for swirl pipe designs. However, a lobate swirl duct cannot be added directly to a cylindrical pipe without incurring wasteful pressure losses. A better solution is to allow the shape to develop in a sigmoidal fashion. A family of sigmoidal coefficients is given by

http://dx.doi.org/10.5772/intechopen.78959

$$\beta\left(\frac{z}{L}\right) = \left[\frac{1 - \cos\left(\pi\frac{z}{L}\right)}{2}\right]^n \tag{37}$$

and illustrated in **Figure 8**.

For a Spanner-type lobate duct, the sigmoidal function can be used to schedule the growth of lobe area, the expansion of the duct or, usually, the development of the radius of the lobe to its final value. In this case, the factors are

$$\beta\left(\frac{L-z}{L}\right) \text{ for entry, } \left\{1 - \beta\left(\frac{L-z}{L}\right)\right\} \text{ for exit} \tag{38}$$

The exponent n governs the steepness of the sigmoidal curve. If $n > 0.5$, the initial gradient is effectively zero, giving a gradual increase in shape.

Originally, a *Three-Zone* development was proposed by Jones and Ariyaratne [12] whereby the entry section was a beta transition with $n = 2$, followed by a fixed-pitch section, followed again by an exit transition with $n = 0.5$. This was certainly an improvement on the system without transitions, but the fixed-pitch section constrained the angular acceleration of the liquid in the duct. Later designs embodied a continuous development of shape and helix. The *symmetric* development had an increasing beta function to the central point of the duct followed by a decreasing beta function to the outlet. The *asymmetric* development had an increasing beta function to a point two-thirds along the length of the duct and a decreasing beta function for the latter third. The asymmetric development gave slightly better swirl intensity results than the symmetric development.

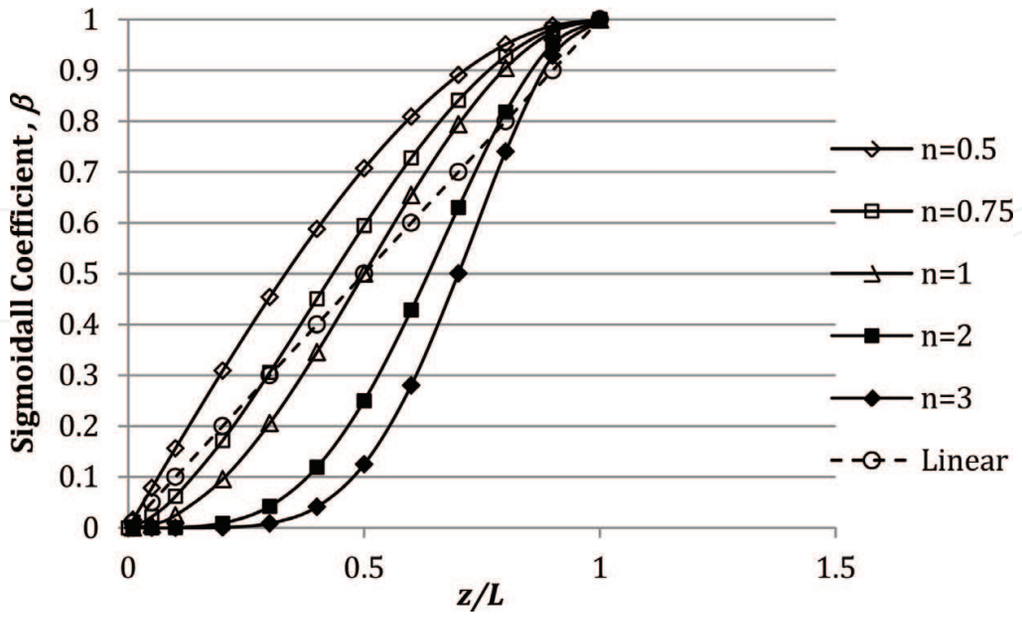

Figure 8. Coefficients for the development of cross-section shape.

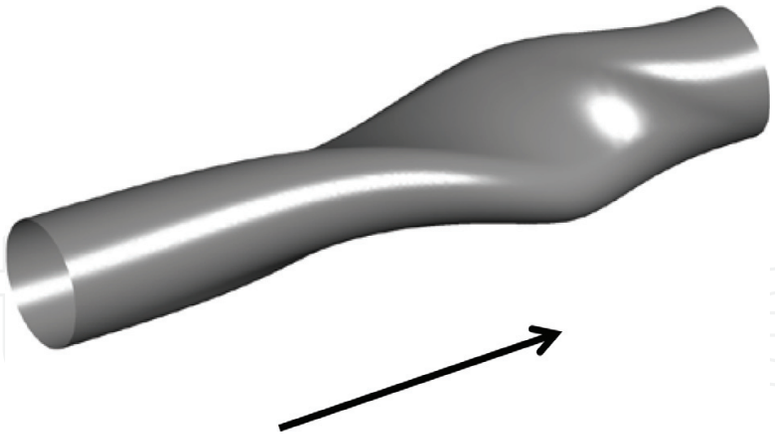

Design variables		Performance	
Upstream diameter	50 mm	Axial velocity	1.5 m/s
Length	300 mm	Reynolds number	74,775
Cross-section	2-lobe	Friction factor[a]	0.0191
Lobe radius	13.8 mm	$\Delta P^{**} =$	333.25 Pa
Shape development	Asymmetric 2:1	Cylindrical tube[c] $\Delta P_s =$	128.6 Pa
Entry sigmoid	$n = 2$	Pressure penalty	2.59
Exit sigmoid	$n = 2$	Swirl intensity at outlet plane[b] (swirl number)	0.0716
Total twist	180°	Swirl effectiveness[b]	0.241
Helix development	$\lambda z + G_0$	[a]Blasius equation for smooth tubes: $f = 0.3162 \times Re^{-0.25}$	
$G_0 =$	0.0	[b]RSM-ω [5]	
$\lambda =$	69.81 rad/m/m	[c]Darcy-Weisbach equation: $\Delta P = f \frac{L}{D} \frac{\rho u^2}{2}$	

Table 2. Design data sheet for a two-lobe swirl inducing duct (lobe radius = 1 × R_4).

4.4. Helix development

Raylor [11] showed that advantages accrued from the gradual angular acceleration of twist in a profiled tube. In recent work, this has been combined with the asymmetric beta function to create a duct with developing cross-sections and acceleration of twist throughout the tube. Inserting the driving function for this case we obtain

$$Tu\frac{dG}{dz} + G = \lambda z + G_0 \tag{39}$$

where λ is the rate of increase of G along the duct, and G_0 is the starting value.

Eq. (16) gives the complementary function as in the previous cases

$$G_{cf}(z) = Be^{-\frac{z}{Tu}} \tag{40}$$

The *particular integral* (PI) is obtained by trying $G(z) = Pz + Q$ in [4] and equating to the ramp function $G_D(z) = \lambda z + G_0$

$$TuP + Pz + Q = \lambda z + G_0 \tag{41}$$

Comparing coefficients we have the solution for the PI

$$G_{pi}(z) = \lambda z - Tu\lambda + G_0 \tag{42}$$

Hence, the complete solution (PI + CF) is given by

$$G(z) = G_{pi}(z) + G_{cf}(z) = \lambda z - Tu\lambda + Be^{-\frac{z}{Tu}} + G_0 \tag{43}$$

Applying the boundary condition $G(0) = G_0$ gives $B = Tu\lambda - G_0$.

So

$$G(z) = \frac{d\theta}{dz} = \lambda z - Tu\lambda + (Tu\lambda - G_0)e^{-\frac{z}{\tau u}} \tag{44}$$

Eq. (44) specifies the response of the solid body model to the ramped driving function in Eq. (39). A two-lobe design is illustrated in **Table 2**. The design is a modestly twisting tube but pressure losses are considerably larger than those expected in a smooth straight duct for the same duty (using the Darcy-Weisbach equation for this prediction). Increasing the amount of twist and increasing the number of lobes to four can improve the performance of the tube at the expense of increased pressure loss.

5. Conclusion

The purpose of this chapter has been to examine the technical aspects of swirling flows and to facilitate the design of ducts for specific purposes. Swirling flow is a complex, while stunningly beautiful, phenomenon and my work has been guided by the need to reduce its complexity for the designer. The emphasis has been on Spanner-type profiled tubes, but this is by no means the only way to generate swirl. The fascinating medical prospect that small amplitude helically coiled pipes might be used as bypass grafts to prevent occlusion by thrombosis has been the subject of scholarly study [14, 15].

The efficacy of the first-order solid body model was demonstrated by the simulation of flow through a 10.0-m cylindrical tube. The prediction that the downstream data taken after a distance of $3Tu$ would be representative of fully developed flow was amply demonstrated. Swirling flows are a little more difficult to predict than by using a simple exponential decay formula, but the solid body model introduced in this chapter is a simple and useful tool to apply to the design task.

Acknowledgements

As always, I am indebted to my research students Benjamin Raylor, Jeyakumar Ganeshalingam, Chanchala Ariyaratne and Ruth Tonkin for their tireless experimental and computational work in the early days. I am particularly indebted to Benjamin Raylor for his continued efforts to the present day, his enthusiasm for swirl ducts, his hard work and unfailing support.

Author details

Trevor Frank Jones

Address all correspondence to: info@tfjconsulting.com

TFJ Consulting Ltd., Derby, England

References

[1] Spanner EF. British Patent GB521548; May 24, 1940

[2] Spanner EF. British Patent GB569000; April 30, 1945

[3] Gordon HM, HA. Conduit or pipe. US Patent 630,605; August 8, 1899

[4] Kitoh O. Experimental study of turbulent swirling flow in a straight pipe. Journal of Fluid Mechanics. 1991;**225**:445-479

[5] ANSYS. Omega Reynolds Stress model. ANSYS CFX-Solver Theory Guide, Release 17. Canonsburg, PA: ANSYS Inc. pp. 95-96

[6] Kolmorogov AN. On degeneration (decay) of isotropic turbulence in incompressible viscous fluids. Doklady Akademii Nauk SSSR. 1941;**31**:538-540

[7] Tonkin RJJ. Swirling pipeflow of non-Newtonian and particle-laden fluids [thesis]. University of Nottingham; 2004

[8] Ganeshalingam J. Swirl induction for improved solid-liquid flow in pipes [thesis]. University of Nottingham; 2002

[9] Steenbergen W, Voskamp J. The rate of decay of swirl in turbulent pipe flow. Flow Measurement and Instrumentation. 1998;**9**:67-78

[10] Halsey DM. Flowmeters in swirling flows. Journal of Physics E: Scientific Instruments. 1987;**20**

[11] Raylor B. Pipe design for improved particle distribution and improved wear [thesis]. University of Nottingham; 1998

[12] Jones TF, Ariyaratne C. Design and optimisation of swirl pipe geometry for particle-laden liquids. AICHE Journal. 2007;**53**(4):757-768

[13] Ariyaratne C. Design and optimization of swirl pipes and transition geometries for slurry transport. University of Nottingham; 2005

[14] Cookson AN. Computational investigation of helical pipe geometries from a mixing perspective [thesis]. London: Department of Aeronautics, Imperial College; 2009

[15] Caro CG, Seneviratne A, Heraty KB, Monaco C, Burke MG, Krams R, et al. Intimal hyperplasia following implantation of helical-centreline and straight centerline stents in common carotid arteries in healthy pigs: Influence of intraluminal flow. Journal of the Royal Society Interface. 2013;**10**. DOI: 10.1098/ rsif 2013.0578

IntechOpen